

White Dwarf Variability

Keaton J. Bell^a

^aCUNY Queens College, Department of Physics, 65-30 Kissena Blvd, Flushing, NY, 11367, USA

© 20xx Elsevier Ltd. All rights reserved.

Keywords: White dwarf stars (1799), Stellar pulsations (1625), Stellar rotation (1629), Ellipsoidal variable stars (455), Asteroseismology (73), ZZ Ceti stars (1847)

Abstract

There are a few different mechanisms that can cause white dwarf stars to vary in brightness, providing opportunities to probe the physics, structures, and formation of these compact stellar remnants. The observational characteristics of the three most common types of white dwarf variability are summarized: stellar pulsations, rotation, and ellipsoidal variations from tidal distortion in binary systems. Stellar pulsations are emphasized as the most complex type of variability, which also has the greatest potential to reveal the conditions of white dwarf interiors.

Key Points

Variations in the brightness of white dwarf stars can reveal details about the physical conditions of these compact stellar remnants:

- Stellar pulsations cause some white dwarfs to vary in brightness at frequencies that are resonant within the star, sensitively probing the conditions of the stellar interior.
- Rotation of white dwarfs can cause brightness variations if the surface is not uniformly bright, enabling the measurement of rotation rates.
- Tidal distortion of white dwarfs in tight binaries can cause ellipsoidal variations when the projected area of the white dwarf varies through the orbit, which can constrain the inclination angle of the system.

Variations from stellar pulsations have the most complicated characteristics:

- A white dwarf pulsates when passing through an instability strip, where the temperature is right given its atmospheric composition for pulsations to be globally driven.
- Not all resonant frequencies are driven to observable amplitude, and the pulsation modes that we observe vary from star to star.
- The pulsations of white dwarfs are non-radial gravity-mode pulsations with buoyancy as a restoring force. On average these pulsations are evenly spaced in period, with variations from even spacing that encode information about interior structure.
- Rotation splits pulsations into multiplets of frequencies that can be represented by different spherical harmonic brightness variations.
- Interactions of pulsation modes with each other or the convection zone can affect the pulse shape, affect coherence of pulsations, or cause sudden brightness increases as pulsation energy is released as pulsational outbursts.

Glossary and Nomenclature

White dwarf stars are the compact objects that remain after most stars exhaust all of their nuclear fuel.

Light curves consist of measurements of stellar brightness recorded at different times.

Periodograms can be computed from light curves to detect and characterize frequencies of brightness variations.

Gravity mode pulsations are stellar oscillations with buoyancy as the restoring force.

Instability strips are atmosphere-dependent combinations of masses and effective (surface) temperatures where pulsations are driven.

DAVs (ZZ Ceti variables) are hydrogen-atmosphere white dwarfs that pulsate with effective temperatures around 10,500–13,000 K.

DBVs (V777 Her variables) are helium-atmosphere white dwarfs that pulsate with effective temperatures around 22,000–31,000 K.

GW Vir stars are pulsating hot white dwarfs or pre-white dwarfs with effective temperatures in the range 80,000–180,000 K.

Asteroseismology is the collection of techniques that are used to interpret pulsation properties to infer stellar parameters.

Ellipsoidal variations are brightness variations caused by tidal distortions of stars in tight binary systems.

1 Introduction

Most white dwarf stars are remarkably constant in brightness over a wide range of timescales (Hermes et al., 2017a). Being photometrically stable makes white dwarfs valuable as flux standards for calibrating (spectro)photometric systems, enabling flux measurements to be converted to physical units. The relative simplicity of modeling pure-hydrogen atmospheres motivates the use of white dwarf stars as calibrators for observations made with the Hubble Space Telescope (Bohlin, 2014), Spitzer (Bohlin et al., 2011), and JWST (Mullally et al., 2022).

However, some white dwarfs make exceptions and vary in brightness in ways that reveal more about their physical properties. Observations that constrain the properties of these objects are astrophysically valuable for multiple reasons, including:

2 White Dwarf Variability

1. White dwarf stars are the final evolutionary state for 97% of stars in the Milky Way (Kalirai et al., 2008). They serve as observational boundary conditions for shaping our understanding of stellar evolution and its effect on planetary systems, especially during the rapid late stages when considerable mass loss occurs.
2. White dwarfs are compact objects, providing remote laboratories for studying the behavior of matter under extreme physical conditions (Saumon et al., 2022; Isern et al., 2022).
3. White dwarfs evolve by cooling, and their temperatures or luminosities can be used to constrain ages of stellar populations (cosmochronology; Winget et al. 1987; Fontaine et al. 2001). They are the progenitors of Type Ia supernovae, which provide a rung in the cosmological distance ladder and reveal the dark energy content of the Universe (Riess et al., 1998).

The quality of astrophysical insights afforded by white dwarfs are limited by our understanding of their structures.

This article is concerned with the most common causes of photometric variability: stellar pulsation (section 2), rotation (3), and ellipsoidal variations in binaries (4). Most of the chapter will discuss pulsations, as this behavior is the most rich and complicated. The characteristics of white dwarf variability are summarized, with references to how we interpret these observations with basic theory. The chapter does not aim to provide a thorough review of the scientific literature, but the references given provide some reasonable entry points. The information in this chapter should be useful for characterizing the type of variability recorded in a white dwarf light curve, as a starting point for more detailed investigation.

1.1 Light curve data and periodogram analysis

This chapter is focused on the causes of brightness variations of white dwarfs, which is really only of interest once we know how to answer the question: is this white dwarf varying in brightness? And if so, what are the characteristics of these variations? The type of data that can answer this question is time series photometry: repeated measurements of the brightness of the star from images collected at different times that constitute a light curve. A light curve includes times of observation, measured flux (often normalized to have a mean of one to represent relative flux), and ideally uncertainties on the flux measurements.

Astronomers have been collecting increasingly more time series observations as telescopes aim to monitor the sky for variability on various timescales. Ground-based surveys are increasingly operating in the time domain, such as ASAS-SN (Kochanek et al., 2017) and ZTF (Bellm et al., 2019), and soon the LSST survey from the Vera C. Rubin Observatory (LSST Science Collaboration et al., 2009), which will extend such studies to much fainter stars. Space missions that were primarily motivated by exoplanet science, such as *Kepler* (Borucki et al., 2010), *K2* (Howell et al., 2014), and TESS (Ricker et al., 2015), have provided precise, continuous light curves with coverage spanning from months to years. The continuous nature of these light curves limits confusion over the timescales of variability that occurs when there are gaps in the data. The value of continuous observations of white dwarf stars motivated the Whole Earth Telescope (Nather et al., 1990) prior to the space photometry era: a collaboration between observatories distributed in longitude that can hand off observations around the globe to maintain coverage despite limited target visibility at each observing site.

With the right data in hand, the question becomes: is this light curve consistent with constant brightness, or has it recorded a significant variation in brightness? The statistical technique used to answer this question most often is periodogram analysis. Based on the Fourier Transform, various periodogram methods transform time domain photometric data into the frequency domain, revealing how much the light curve varies at different frequencies. This transformation decomposes the light curve into a set of sinusoidal basis functions, each with a different frequency. Plotted for a series of tested frequencies (or sometimes their reciprocal: periods), periodograms show either the best-fit amplitude of a sinusoid at each sampled frequency, or the power, which is the square of the amplitude. Examples of periodograms for five pulsating hydrogen-atmosphere white dwarfs are displayed in the bottom panels of Fig. 1, where amplitude of variability is displayed in percent, and frequency is given in microHertz ($1 \mu\text{Hz} = 10^{-6} \text{ Hz} = 10^{-6} \text{ second}^{-1}$). Fourier methods can reveal signals that are not immediately apparent when visually inspecting a light curve, because the signal amplitudes may be smaller than the per-point measurement noise. In the periodogram, measurement noise gets distributed across all frequencies, while brightness variations appear as peaks that rise significantly above this noise floor at particular frequencies, which can be identified with statistical methods (VanderPlas, 2018).

Accurate period measurements are most reliably determined from continuous light curves that are rapidly sampled. Gaps in data and low-frequency sampling (such that signals are sampled fewer than twice per period, i.e., above the Nyquist frequency) introduce signal aliases to periodograms (VanderPlas, 2018), like reflections of the true signals at inaccurate frequencies. This article will focus on high-cadence, nearly continuous data from space where these issues are largely avoided.

2 White dwarf pulsations

Some white dwarf stars pulsate. If their conditions are just right, they will oscillate globally at one or more natural frequencies that are resonant within the star. Pulsation periods are typically in the range 2–20 minutes, with relative amplitudes of photometric variations observed to range from parts per thousand up to ten percent (Mukadam et al., 2006). The pulsations compress the stellar material, causing temperature and corresponding brightness variations at the photosphere. Resonant frequencies of the star can be measured from light curves via periodogram analysis (1.1). This enables these white dwarfs to be studied with the powerful techniques of asteroseismology: the analysis of resonant frequencies to infer properties of the stellar interior. The pulsations propagate through the white dwarf, and their frequencies are sensitively tuned by the precise structure of the star. Asteroseismic interpretation of pulsation signals has the potential to probe white dwarf interior structures and physics, which have important astrophysical consequences. The most common approach to inferring interior structures of white dwarfs is by forward modeling, whereby pulsation periods calculated from numerical models of white dwarfs with different structures are fit to the observed pulsation periods (e.g., Giammichele et al., 2022). We discuss the main classes of pulsating white dwarf, with a focus on the most populous “DAV” class where observational trends have been most clearly established.

2.1 Driving of pulsations in the instability strips

A small subset of white dwarf stars are pulsating—those with just the right conditions that oscillations are self-driven and amplified by the stellar interior. White dwarfs that meet these conditions for pulsations are within pulsational “instability strips”—regions of observational parameter space

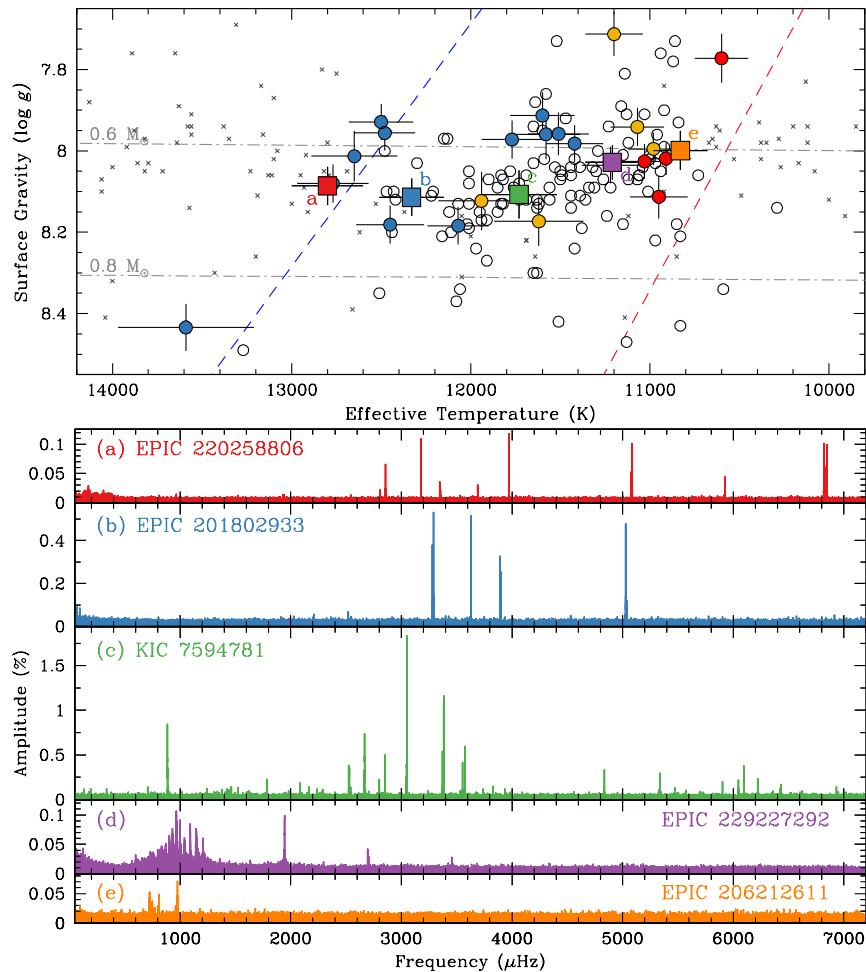


Fig. 1 Examples of DAVs observed by *Kepler/K2* at different temperatures across the instability strip (Hermes et al., 2017b). The top panels shows where DA white dwarfs pulsate in the spectroscopic parameter space of \log -surface-gravity ($\log g$) and effective temperature. Circle and square markers indicate the parameters of some pulsating DAV stars. Small crosses show white dwarfs not observed to vary, but within the instability strip this is likely due to insufficient signal-to-noise of the data. Dash-dotted lines show how models of white dwarfs of masses $0.6 M_{\odot}$ and $0.8 M_{\odot}$ cool across the parameter space. The blue and red edges of the instability strip are marked with dashed lines. Red circles indicate outbursting DAVs (Section 2.5).

The bottom panels display the periodograms of the *Kepler/K2* light curves of, from top to bottom, five progressively cooler DAVs. Their locations in the instability strip are indicated with square markers of corresponding color and letter in the upper plot. As DAVs cool across the pulsational instability strip, they tend to drive pulsations with progressively longer periods (lower frequencies). The higher-frequency modes appear as sharp features in the periodogram, indicating a high degree of coherence, while low frequency modes ($\lesssim 1250 \mu\text{Hz}$) are less coherent, with power smeared across sampled frequencies (Section 2.4). The highest amplitudes are observed near the middle of the instability strip.

© AAS. Reproduced from Hermes et al. (2017b) with permission.

where white dwarfs are observed to pulsate. There are three primary instability strips for white dwarfs, and white dwarfs that pulsate in each of these regimes are classified as either DAVs, DBVs, or GW Vir stars. The main classes of pulsating white dwarfs and their respective driving mechanisms are described below.

The driving mechanism is responsible for exciting some vibrational modes of a star to observable amplitude. The driving mechanisms operating in white dwarfs are not perfectly understood; it is unknown why only select pulsation modes are excited in individual stars, while other modes with similar characteristics are not detected (e.g., Castanheira et al., 2013). Fortunately, the specifics of the driving mechanism do not have much bearing on the interpretation of detected pulsation frequencies. However the modes are driven, they reveal some of the resonant frequencies of the pulsating stars, which can be studied to infer details of their interior structures.

2.1.1 DAVs: hydrogen-atmosphere pulsating white dwarfs (ZZ Ceti stars)

Hydrogen-atmosphere white dwarf stars, known as DA white dwarfs, are observed to pulsate when their effective temperatures fall between 10,500–13,000 K (Hermes et al., 2017b). The pulsating DAs are called DAVs (“V” for “variable”), or ZZ Ceti stars after one of the earliest DAVs discovered (Lasker and Hesser, 1971). The hot and cool limits of the instability strip are referred to as the blue and red edges. As a DA white dwarf

4 White Dwarf Variability

cools to the temperature of the blue edge, electrons in the atmosphere are able to recombine with hydrogen nuclei, increasing the opacity and impeding the outward flow of radiation sufficiently to establish an outer convection zone, which deepens as the star cools further. The pulsations are understood to be driven to observable amplitude by the convective driving mechanism, where the convection zone absorbs and releases energy in response to local radiative flux variations in a way that amplifies oscillations (Brickhill, 1991; Goldreich and Wu, 1999).

DAVs are the most populous class of pulsating white dwarf, with around 500 known examples (Romero et al., 2022). The boundaries of the instability strip are mass dependent, with more massive white dwarfs pulsating at higher temperatures (Kilic et al., 2023), and low-mass white dwarfs pulsating at cooler temperatures (Hermes et al., 2013; Van Grootel et al., 2013). A sample of DAVs, and the blue and red edges of the instability strip, are shown in the spectroscopic parameter space of effective temperature and log surface gravity in the top panel of Fig. 1 (where higher surface gravities correspond to more massive white dwarfs).

With a large sample of DAVs available for study, observational trends across the instability strip are well established (Mukadam et al., 2006; Hermes et al., 2017b). Observations support that the DAV instability strip is “pure,” in the sense that all white dwarfs with hydrogen atmospheres are expected to pulsate as they cool through this region of parameter space (Bergeron et al., 2004; Castanheira et al., 2007); therefore asteroseismic inferences about the structures of DAVs are representative of DA white dwarfs generally. As DA white dwarfs cool across the instability strip, they are observed to pulsate with progressively longer periods on average. As the depth of the convection zone increases as a white dwarf cools, its thermal timescale increases, and the convective driving mechanism can more efficiently drive modes with longer periods (Wu and Goldreich, 1999). Pulsators near the middle of the strip are observed to exhibit the highest-amplitude variability. These trends are visible in the lower panels of Fig. 1, which compare periodograms of progressively cooler DAVs. Distinctions in the relative coherence of modes with different pulsation timescales are described in 2.4, and the outburst behavior observed near the red edge of the instability strip is detailed in 2.5.

2.1.2 DBVs: helium-atmosphere pulsating white dwarfs (V 777 Her stars)

Helium-atmosphere white dwarf stars are called DB white dwarfs, and the variables are DBVs. These stars are observed to pulsate when their effective temperatures fall between 22,000–31,000 K (Vanderbosch et al., 2022). DBVs are sometimes called V 777 Her stars after their prototype (Winget et al., 1982a). By analogy to DAVs, which pulsate at effective temperatures where a partial ionization of hydrogen first establishes an outer convection zone, the DBs were theoretically predicted to pulsate at higher temperatures where the helium atmosphere becomes partially ionized (Winget et al., 1982b). This allows convection to drive pulsations as it does for DAVs (Van Grootel et al., 2017). There are around 50 DBVs known to date (Córscico et al., 2022), and their observed mode characteristics across the DBV instability strip generally mimic the behaviors of DAVs (Vanderbosch et al., 2022).

2.1.3 GW Vir stars: hot pulsating white dwarfs and pre-white dwarfs

Following the ejection of their outer layers as planetary nebulae, the remnant cores of dying stars contract onto the white dwarf cooling track as PG 1159 stars. Many of these are observed to pulsate as “GW Vir” stars with effective temperatures in the range 80,000–180,000 K (Sowicka et al., 2023). The GW Vir instability strip has been referred to as the “DOV” instability strip, and some pulsating stars still enshrouded in planetary nebulae have been called PNNVs, for “planetary nebula nucleus variables.” Stars cross this instability regime twice, once as they are contracting and increasing in effective temperature, and then again as they begin cooling at the hot end of the white dwarf cooling track. Unlike the DAV and DBV classes, not all stars in the GW Vir instability strip are observed to pulsate; only around 1/3 of stars in the mass– T_{eff} space of the GW Vir instability strip pulsate (Sowicka et al., 2023), and those with more nitrogen in their atmospheres are more likely to show detectable variability (Sowicka et al., 2021). These hot white dwarfs do not have outer convection zones, and their pulsations are driven by the kappa-gamma mechanism operating on the K-shell electrons of carbon and oxygen (Saio, 1996; Gautschy et al., 2005). There are two dozen GW Vir pulsators known to date (Uzundag et al., 2022).

2.2 Nonradial gravity mode oscillations

Each resonant frequency of the star corresponds to a different mode of oscillation, and pulsating white dwarfs typically oscillate in many modes simultaneously. The pulsations observed from white dwarf stars are theoretically and observationally (Robinson et al., 1982) consistent with gravity mode oscillations (g-modes), where displacements within the star are restored by buoyancy. As opposed to pressure modes (p-modes), which are the other most common type of stellar pulsation observed in other types of star (including the Sun), gravity modes have longer periods and involve mostly horizontal displacements (Aerts et al., 2010). Gravity modes have specific characteristics that can guide the interpretation of detected pulsation signals (2.2.3).

The discrete set of pulsation modes of a spherical star are three dimensional, and the oscillations are characterized with three quantum numbers: k , the radial overtone number (called n in some areas of asteroseismology); ℓ , the spherical degree; and m , the azimuthal order. All g-modes are non-radial oscillations, and every mode has an angular dependence that takes the pattern of spherical harmonics for a spherical star (2.2.1), which are described by ℓ and m . The number k describes the radial dependence, and the oscillation frequencies that will be resonant within a star can be best understood from propagation diagrams (2.2.2).

2.2.1 Spherical harmonics

The patterns of pulsations at the stellar surface are spherical harmonics. Spherical harmonics are identified by two quantum numbers: the spherical degree, ℓ , says how many nodal lines are on the surface, and the azimuthal order, m , says how many of these pass through the (rotational) poles of the star. The spherical harmonics for $\ell = 1$ and 2 are shown in Fig. 2. White dwarfs typically pulsate in many modes simultaneously, each taking the form of a spherical harmonic oscillating with its own frequency and amplitude.

Spherical degree (ℓ)

For nonradial oscillations, ℓ is an integer of one or greater. For higher ℓ , the surface of the star gets sliced into increasingly many small sectors, and for each patch of the surface that is getting brighter during a pulsation cycle, there is a neighboring region that is getting darker. When observing the disc-integrated light from a star, adjacent regions tend to cancel each other out when there are a large number of nodal lines on the surface

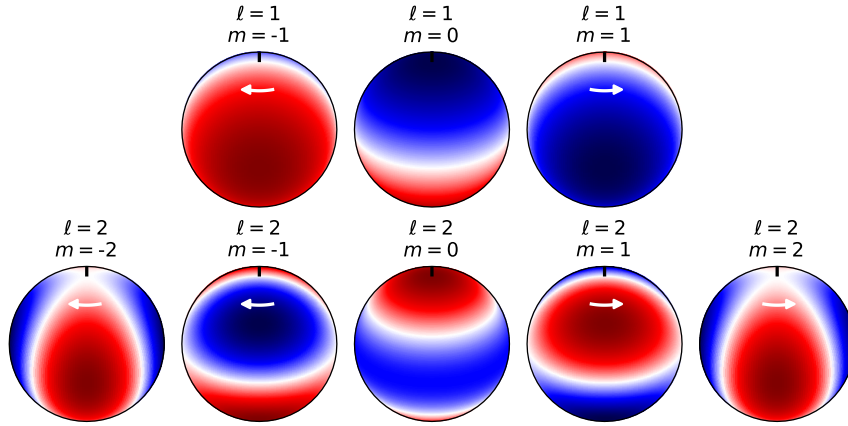


Fig. 2 Spherical harmonic patterns of stellar pulsation for $\ell = 1$ and 2 modes that are observed from pulsating white dwarfs. The $m = 0$ modes are standing waves on the surface that oscillate in place. The $m \neq 0$ modes are traveling waves moving in opposite directions on the surface depending on the sign of m , as indicated with the white arrows. Maps are displayed with a 60 degree inclination, and the rotational poles are marked with black lines.

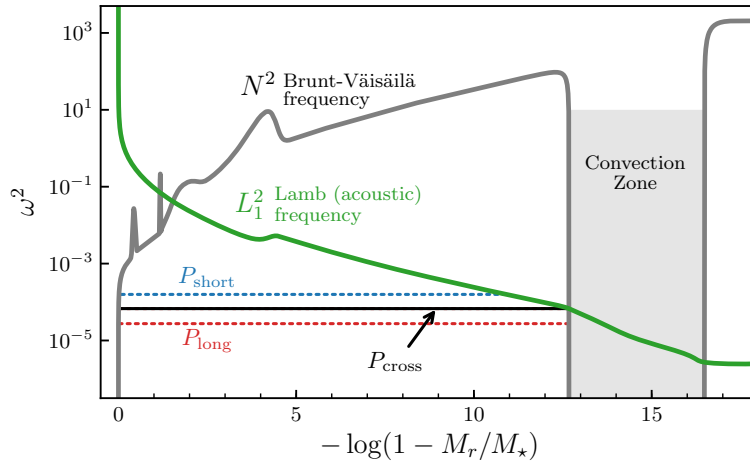


Fig. 3 A propagation diagram from a stellar model of a DAV pulsator. See section 2.2.2 for discussion. © AAS. Reproduced from Montgomery et al. (2020) with permission.

(Dziembowski, 1977), and pulsation signals observed from white dwarfs are usually assumed to be $\ell = 1$ or $\ell = 2$ modes.

Azimuthal order (m)

The number of the ℓ nodal lines on the stellar surface that pass through the poles is recorded as m . For white dwarfs, the poles are typically thought to correspond to the rotation axis. If $m = 0$, all ℓ nodal lines slice through the star parallel to the equatorial plane. This separates the surface into neighboring regions that vary in brightness as a standing wave, each in anti-phase to its neighbors. If $m \neq 0$, the patterns shown in Fig. 2 appear as traveling waves on the surface. Whether m is positive or negative determines whether the spherical harmonics travel in the prograde or retrograde direction with respect to rotation, and it must be the case that $|m| \leq \ell$.

2.2.2 Propagation diagrams

To understand the radial dependence of white dwarf pulsations, it is useful to consider propagation diagrams like the one displayed in Fig. 3. Propagation diagrams are a representation of the physical properties of a stellar model that are relevant to tuning the pulsation frequencies. They show how the characteristic Brunt-Väisälä (BV) and Lamb frequencies vary through the stellar model from center (left) to surface (right). The BV frequency is the frequency at which a displaced portion of the star would oscillate about its equilibrium position at different depths within the star due to buoyancy, and the Lamb frequency is a characteristic acoustic frequency (with dependence on ℓ). These are commonly plotted against mass coordinate for white dwarfs written as $-\log(1 - M_r/M_*)$, where a number X on the x-axis means that 10^{-X} of the star by mass is to the right of that point on the diagram; this makes details of the thin white dwarf envelope discernible in graphs.

Regions of transition in the properties of the stellar model impart signatures in the characteristic frequencies. In Fig. 3, local bumps in the BV frequency can be identified to correspond to the base of the hydrogen envelope ($-\log(1 - M_r/M_*) = 4$), the base of the helium layer ($= 2$), and at

steep gradients in the carbon/oxygen ratio within the core. Gravity waves cannot propagate into a convective region, so the BV frequency drops sharply to zero at the base of the convection zone.

The gravity modes observed in white dwarfs oscillate in regions of the star below both the BV and Lamb frequencies. No pressure mode pulsations have been definitively detected from a white dwarf. The resonant frequencies of the gravity modes are tuned such that the oscillations just fit in the cavity below the BV and Lamb frequencies, with k nodes in between. Modes with higher radial overtone number, k , oscillate with longer periods (lower in the propagation diagram). The resonant pulsation frequencies of white dwarfs are acutely sensitive to local features in the BV and Lamb frequencies, and therefore provide a powerful diagnostic for inferring the details of white dwarf interior structures.

2.2.3 Mean period spacing and deviations

A useful property of gravity modes is that, in the asymptotic limit of high radial overtone number, k , successive radial overtones are evenly spaced in period (Aerts et al., 2010). That statement applies to axisymmetric ($m = 0$) modes of the same ℓ value. For $k \gg \ell$, the spacing between $m = 0$ pulsation periods of subsequent k is, on average,

$$\Delta\Pi_\ell^a = \frac{\Pi_0}{\sqrt{\ell(\ell+1)}}, \quad (1)$$

where Π_0 is a constant.

The behavior in the asymptotic limit is an idealization, and real white dwarf pulsation modes are observed (and calculated) to roughly align with an even period spacing on average (for $k \gg \ell$). The ‘‘mean period spacing’’ is most sensitive to the global stellar parameters of mass and effective temperature, though other parameters also have some influence (H layer mass in DAVs, especially; Tassoul et al. 1990). Identifying the pattern of average spacing in a set of measured pulsation periods can constrain these global properties, and can guide the further interpretation of the individual modes. A few statistical techniques commonly used to identify potential mean period spacings are the Kolmogorov–Smirnov (Kawaler, 1988), Inverse Variance (O’Donoghue, 1994), and Fourier Transform (Winget et al., 1991) tests.

The deviations from a perfectly even period spacing carry information about aspects of the stellar interior structure that cause localized features in the BV and Lamb frequencies. A useful analogy can be made to the pattern of standing waves on a string (Montgomery, 2005b). For a string of uniform density, the frequencies of successive overtones are separated by an equal amount, in the same way that g-modes in a smooth, idealized star have an even period spacing. However, if the string is not uniform, and has one or more localized regions where the wave speed changes, the pattern of overtones will depart from the even spacing in frequency, though the deviations will vary about an even average spacing. The same happens in a white dwarf due to bumps in the BV frequency. Any localized feature will modify the resonant wave functions by an amount that depends on its location relative to the radial nodes. The deviations about the mean period spacing are cyclic, and the pattern of deviations is known as the mode trapping cycle. The specifics of these deviations are decided by the specifics of the localized features in the propagation diagram, and therefore the individual mode periods carry information about the precise interior structure profile of a pulsating white dwarf star (C3rscico et al., 2002).

2.2.4 Rotational splittings

In a spherically symmetric star, the spherical harmonics of different m are degenerate. Rotation of a white dwarf can lift this degeneracy, splitting modes of each ℓ and k into $(2\ell + 1)$ components with different frequencies. In the slow-rotating limit, these rotationally split modes are separated in frequency from the $m = 0$ mode by an amount

$$\delta\nu_{k,\ell,m} = m(1 - C_{k,\ell})\Omega \quad (2)$$

where Ω is the rotation frequency, and $C_{k,\ell}$ are the Ledoux constants that describe the effect of the Coriolis force on the modes (Ledoux, 1951). For gravity modes, $C_{k,\ell}$ asymptotically approaches $1/(\ell(\ell+1))$ in the limit of high k , and it is generally less than this value below the asymptotic limit.

Identification of rotational multiplets in the periodograms of white dwarfs can reveal white dwarf interior rotation rates. Hermes et al. (2017b) found that more massive white dwarfs have generally faster rotation rates, evidenced by the larger splittings of rotational multiplets. Figure 4 shows examples of rotational $\ell = 1$ triplets identified in periodograms of TESS light curves from Bogn3r and S3dor (2024).

Rotational splittings also aid in mode identification, as $\ell = 1$ modes are split into triplets, and $\ell = 2$ modes are split into quintuplets with a different frequency spacing. However, it is not common for all components of rotational multiplets to be driven to observable amplitudes in white dwarfs, and most observed modes are not clearly part of multiplets. In the absence of observing sufficient multiplet components to make clear m identifications, asteroseismic analyses should avoid assumptions about the m value of observed modes.

2.3 Nonlinear pulsations

The structure of the white dwarf can adjust dynamically to the stellar pulsations, and since the pulsations all interact with the star, nonlinear effects can arise. In DAVs and DBVs, the pulsations are driven by the convection zone, and the convection zone adjusts on a timescale much faster than the pulsation timescale. As a result, the convection zone varies in depth in response to local variations in temperature. The deeper the convection zone, the more the pulsation signals are attenuated at the photosphere. During a pulsation cycle, the outflowing energy reaches the photosphere more readily through hot regions of the star, where the convection zone is locally thinner. This causes the photometric variations due to pulsations to not be strictly sinusoidal, but to have sharper peaks at maximum brightness (Brickhill, 1992).

Modeling the pulsation/convection interaction can aid with mode identification and provides an avenue to study the physics of stellar convection. For a pulsation that is sinusoidal at the base of the convection zone, Montgomery (2005a) shows how modeling the absorption of energy by the convection zone can produce non-sinusoidal flux variations at the photosphere that match observations. The precise shape of pulsation signals in the light curve is determined by how sensitively the depth of the convection zone responds to the pulsations. Montgomery (2005a) parameterize this sensitivity in terms of the thermal response timescale of the convection zone, τ_C ,

$$\tau_C = \tau_0 \left(\frac{T_{\text{eff}}}{T_{\text{eff},0}} \right)^{-N} \quad (3)$$

where T_{eff} is the local effective temperature that varies due to pulsations, and $T_{\text{eff},0}$ and τ_0 are average effective temperatures and thermal response

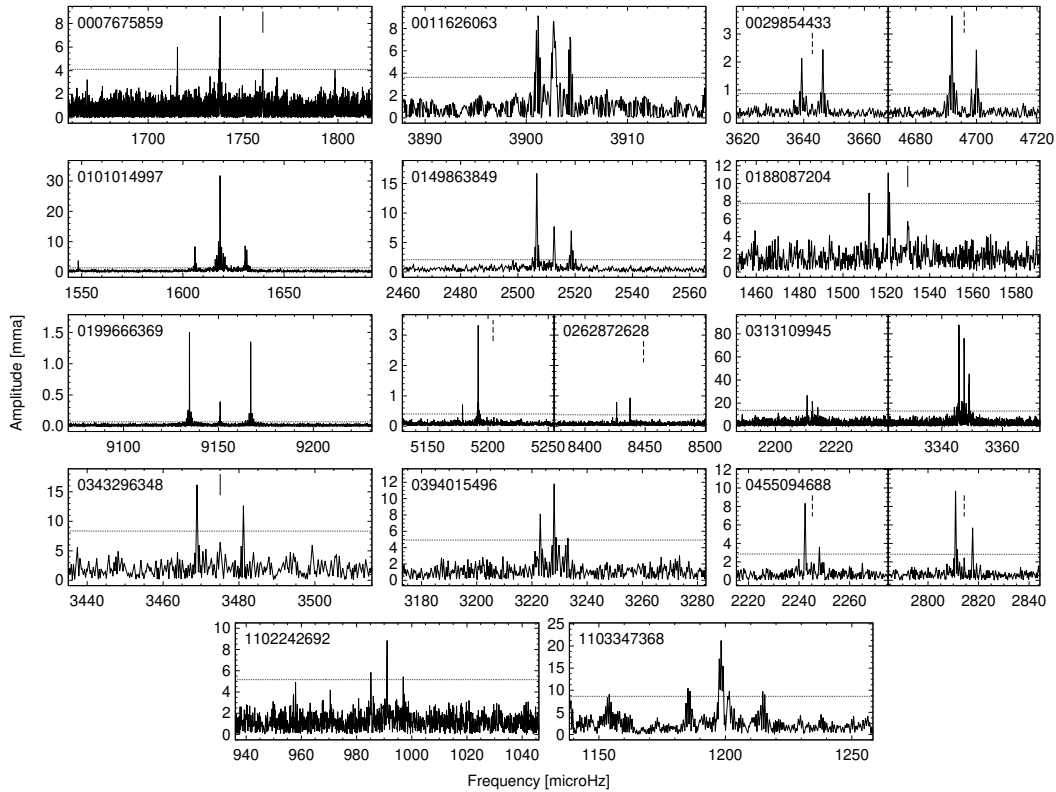


Fig. 4 Examples of rotational splittings of $\ell = 1$ modes in DAV pulsators observed with TESS, from Bognár and Sódor (2024, reproduced with permission from the authors). Dotted horizontal lines shows the significance threshold used in that work to identify signals that are significantly above the noise. Solid vertical markers show where candidate components of the triplets are below the significance threshold, and dotted vertical lines show periods measured from previous observations.

timescales of the convection zone. The exponent N captures how rapidly the convection zone changes in size due to local temperature variations; mixing length theory and fits to light curves say that the response is highly sensitive, with typical values as large as $N \approx 90$ and ≈ 23 in the DAV and DBV instability strips, respectively (Montgomery, 2005a). The results are dependent on viewing angle (inclination) and the spherical harmonic pattern observed (ℓ and m), which nonlinear pulse shapes can also constrain.

Fourier-transform-based periodograms decompose light curves into sinusoids, and nonsinusoidal pulsations will show up as a series of harmonics. The harmonics are at exact integer multiples of the pulsation frequency and combine to reproduce the pulse shape (as a Fourier series). For multiperiodic pulsators, there are additional combination frequencies that appear at precise sums and differences between independent pulsation frequencies. It is essential to white dwarf asteroseismology to identify the periodogram peaks associated with combination frequencies and harmonics, so as not to interpret them as independent resonant frequencies of the star. Once identified, the amplitudes and phases of combination frequencies can aid in mode identification (Wu, 2001; Yeates et al., 2005).

2.4 Mode coherence

Some white dwarfs appear to pulsate in an incredibly coherent fashion, with pulsation signals phasing up over years of observations (Kepler et al., 1982). The pulsation modes of other white dwarfs can change dramatically in phase and amplitude on timescales of days, often looking like completely different pulsators from one observing run to the next (Kleinman et al., 1998). The distinction between these behaviors has reinforced an appreciation for the interactions between pulsations and the convection zone, while the most coherent signals provide opportunities to probe the extreme physics of white dwarfs and the presence of orbiting planets.

2.4.1 A dichotomy of coherence

Before the advent of precision survey photometry from space missions like *Kepler* and TESS, a distinction was noted in the behavior of pulsating white dwarf stars. In DAV pulsators, this difference in behavior was initially interpreted as a temperature effect: hot DAVs near the blue edge of the instability strip tend to have coherent pulsations, and cool DAVs near the red edge are incoherent pulsators (Mukadam et al., 2006).

Continuous high-cadence monitoring from space has clarified the picture. In the periodogram of a continuous time series, the signature of a coherent signal is one sharp, dominant peak. On the other hand, signals that are not coherent on timescales shorter than the span of observations will appear as wide bands of power distributed around a central frequency. These incoherent modes look similar to solar-like oscillations, which are

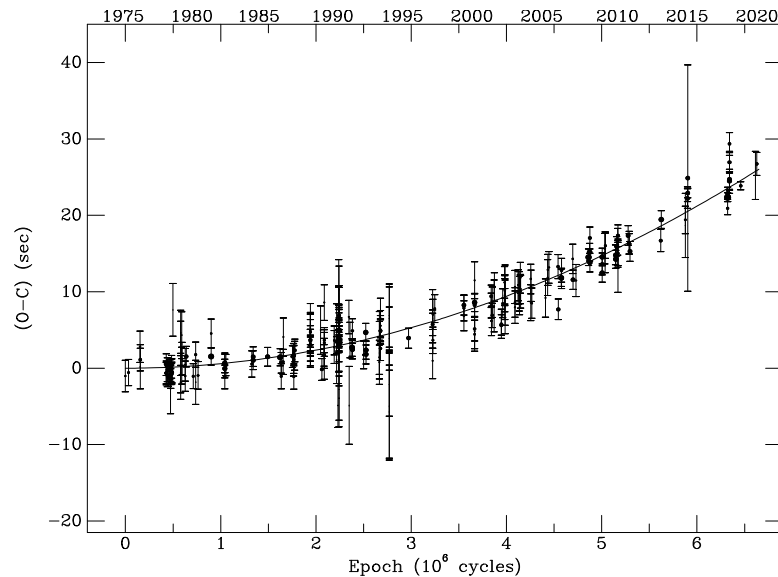


Fig. 5 The observed-minus-calculated ($O - C$) diagram for the 215-second mode of the DAV pulsator G 117-B15A shows a gradual drift corresponding to a rate of period change of $(5.12 \pm 0.82) \times 10^{-15} \text{ s s}^{-1}$. The top axis shows year of observation, and the bottom axis shows the number of pulsation cycles elapsed ($\times 10^6$). © AAS. Reproduced from Kepler et al. (2021) with permission.

stochastically driven and damped by convection, and they can be fit with Lorentzian functions in the power spectrum as is commonly done for solar-like oscillators (Bell et al., 2015).

The work of Hermes et al. (2017b) found that higher frequency pulsations in white dwarfs tend to be coherent, while lower frequency modes are typically incoherent. This can be seen in the bottom panels of Fig. 1, where pulsations with periods shorter than $\approx 800 \text{ s}$ (frequency $\gtrsim 1250 \mu\text{Hz}$) appear as sharp peaks, while power from modes with longer periods is smeared through a small range of sampled frequencies. While the temperature of the star determines which modes are most likely to be excited, both coherent and incoherent modes can coexist within the same star (e.g., panel d of Fig. 1).

Montgomery et al. (2020) provided a physical interpretation of the $\approx 800 \text{ s}$ timescale that separates the pulsation mode behavior into a dichotomy of coherence. In the propagation diagram shown in Fig. 3, this timescale is labeled as P_{cross} , where the BV frequency crosses the Lamb frequency at the base of the convection zone. Pulsation modes with periods shorter than P_{cross} are bounded by the Lamb frequency at their outer turning point, while longer-period modes propagate to the BV frequency that is defined by the base of the convection zone. As described in 2.3, the base of the convection zone in a pulsating white dwarf varies in depth dramatically in response to local temperature variations from the pulsations, causing the size of the resonant cavity to vary. The long-period modes are therefore reflecting from a continuously moving boundary, likely disrupting the coherence of these modes.

2.4.2 Monitoring coherent modes

Unlike the low-frequency modes that are constantly jostled by the convection zone, high frequency pulsations propagate rather undisturbed, deeper within the star. These modes are exceedingly coherent, and some have been subject to decades-long monitoring to track gradual drifts of their pulsation signals. Over 45 years of observations of the 215-second mode in G 117-B15A support that this pulsating white dwarf is the most stable optical clock known (Kepler et al., 2021).

Even the most coherent white dwarf pulsations are not expected to be perfectly steady. White dwarfs evolve by cooling, and the subtle changes to their interior structures while they cool within the pulsational instability strips causes their resonant frequencies to drift slowly. Measuring the rate of pulsation period change (\dot{P}) sensitively tracks the rate of this secular cooling process. Measurements of white dwarf cooling rates can constrain exotic physics that could affect this process, such as the rate of change of the gravitational constant G , the magnetic moments of neutrinos, and properties of WIMPs and axions—both candidate dark matter particles (Isern et al., 2022).

Rates of pulsation period change are typically measured by tracking phase variations of the pulsation signals. An observed-minus-calculated ($O - C$) diagram shows the difference between measured arrival times of pulse maximum and the expected arrival times calculated with the assumption that the signal is strictly periodic (Robinson, 2016, Ch. 9.6). The $O - C$ diagram for the DAV pulsator G 117-B15A from Kepler et al. (2021) is displayed in Fig. 5. Relative to the signal phase when observations began in 1974, observed brightness maxima from pulsation of the 215-s mode have been gradually delayed, by only as much as 26 seconds over 45 years of observations. Because changes compound over time, the signature of a constant rate of period change in an $O - C$ diagram is a parabola. The measured rate of period change of this pulsation mode is $(5.12 \pm 0.82) \times 10^{-15} \text{ s s}^{-1}$ (Kepler et al., 2021), with similar rates measured for other DAVs (Mukadam et al., 2013; Sullivan and Chote, 2015), and faster rates of cooling detected for hotter DBV (Redaelli et al., 2011) and GW Vir (Costa and Kepler, 2008) pulsators.

Another useful aspect of the coherence of high-frequency pulsations in white dwarfs is their potential to reveal orbital companions. If a white dwarf is orbited by a planet, the white dwarf will exhibit a reflex motion about the center of mass of the system. As this reflex motion modulates the distance to the white dwarf along our line of sight, pulsation signals will have to travel different amounts of time to reach our telescopes. Variations in light travel time from a white dwarf experiencing reflex motion produces phase variations that would appear sinusoidal (for a circular orbit) in an $O - C$ diagram. Since most stars end their lives as white dwarfs (Kalirai et al., 2008), and most stars host exoplanets (Kunimoto and Matthews,

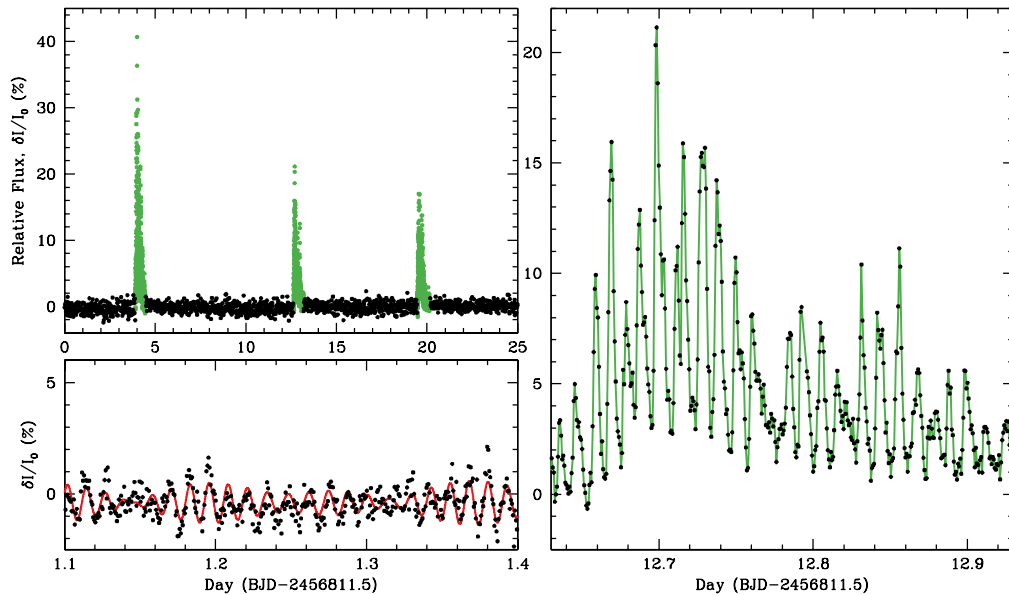


Fig. 6 Portions of the *K2* light curve of the DAV pulsator PG 1149+057. The bottom left panel zooms in on a region of the light curve in quiescence, and the right panel reveals the detailed changes that occur during one outburst. Figure reproduced from Hermes et al. (2015) with permission.

2020), we expect that most white dwarfs host exoplanets (Veras and Gänsicke, 2015; Andryushin and Popov, 2021). So far, attempts to detect exoplanets orbiting white dwarfs from phase modulations of pulsation signals has only yielded upper limits (Mullally et al., 2008; Winget et al., 2015).

2.5 Pulsational outbursts

Some pulsating white dwarf stars have been observed to show dramatic brightness increases that recur on timescales of days and last for many hours. This behavior was first identified in nearly continuous coverage of a DAV from *Kepler* (Bell et al., 2015). These “pulsational outbursts” have only been observed in pulsating DA white dwarfs near the cool edge of the DAV instability strip (some are marked with red circles in Fig. 1), where the behavior appears to be fairly common (Bell et al., 2016). In hindsight, the “whoopsie” or “sforzando” observed in 1996 from the DBV star GD 356 (Kepler et al., 2003; Provencal et al., 2009) was likely the first recorded example of a pulsational outburst from a white dwarf. Fig. 6 shows portions of the *K2* light curve of the outbursting DAV PG 1149+057 (from Hermes et al., 2015). During the outbursts, which can raise the mean brightness of the white dwarf by tens of percent, the pulsations also show an increase in observable amplitude.

An understanding is emerging about the mechanism that causes these outbursts. Somehow, the pulsational energy that builds in the self-driven pulsation modes is rapidly deposited into the outer layers of the star. It has been proposed that a driven pulsation couples to two other, globally damped modes through a parametric resonance; when the amplitude of the driven mode exceeds some threshold, it triggers a transfer of pulsational energy to the globally damped “daughter” modes (Luan and Goldreich, 2018). The temperature rises at the photosphere, causing an overall brightness increase as the star radiates away this excess energy. The convection zone responds to the temperature increase by getting thinner, attenuating remaining pulsation modes by a lesser amount, causing them to temporarily have higher observable amplitudes. Returning to the quiescent state, the driven modes start to build back up in amplitude, and the cycle begins again.

3 White dwarf rotation

Some white dwarf stars are not uniformly bright across their photospheres. Such stars can exhibit photometric variability as rotation brings different parts of the surface into view. This enables surface rotation rates to be measured, as can be done for some other types of star. Suspected causes of rotational photometric variation in white dwarfs include nonuniform accretion of metals (Dupuis et al., 2000), or magnetic field geometries that cause different amounts of local magnetic Zeeman line splitting at the photosphere (Hardy et al., 2023).

Rotational photometric variations are not always simply sinusoidal, and a periodogram can reveal multiple harmonics of the rotation frequency to represent the rotation profile. The underlying rotation frequency does not always have the highest amplitude; if the star has two bright/dark regions on opposite sides of its rotating surface, its dominant photometric variation will be at double the rotation frequency. Depending on the signal-to-noise ratio of your observations, there may not be a significant periodogram signal at the true rotation rate, and only the second harmonic might be detected. This is a challenge for stellar rotation studies of many types of star, and it is good to be aware that the dominant periodogram peaks from rotational variability will sometimes correspond to half the rotation period.

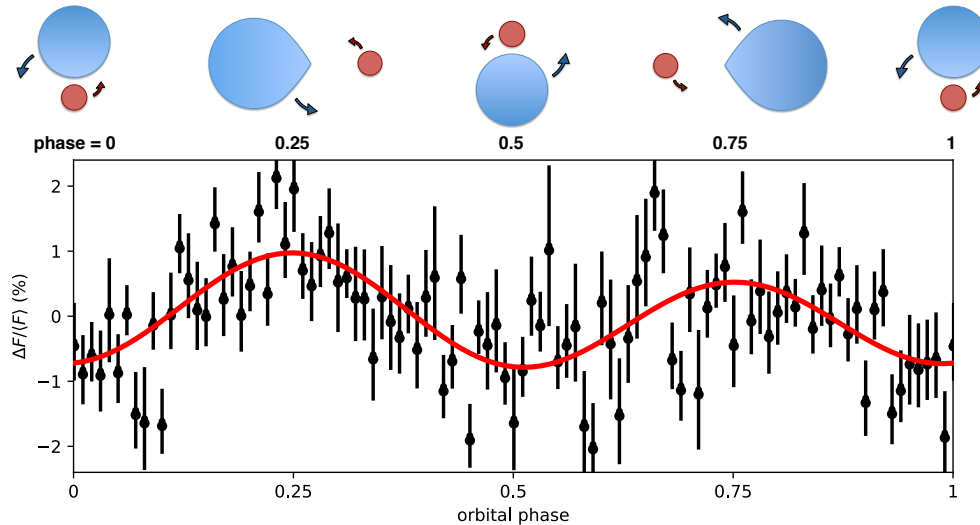


Fig. 7 A cartoon shows (not to scale) how tidal deformation of the extremely low-mass white dwarf primary of the binary system SDSS J1054–2121 corresponds to its photometric variability folded on the 2.5-hour orbital period. Reproduced from Bell et al. (2018).

4 Compact binaries

Many white dwarf stars are found in binary systems, and there are a variety of ways that these systems can be photometrically variable. White dwarfs in binaries can eclipse and be eclipsed, there can be reflection effects, white dwarfs can gravitationally microlens their companions (Kruse and Agol, 2014), mass transfer onto white dwarfs through an accretion disk in cataclysmic variables can produce variability, this accreted material can ignite as novae, and enough mass transfer onto a white dwarf can overwhelm electron degeneracy pressure causing the star to explode as a Type Ia supernova. While all of great scientific interest, these processes are outside the scope of this chapter. We close by discussing one of the more common sources of photometric variability in binary systems: ellipsoidal variations from tidal distortion.

4.1 Ellipsoidal variations in tight binary systems

When two stars in a binary system are very close to each other, the tidal forces can be sufficient to distort the shape of one or both stars. The distortion of the star is aligned along the tidal axis connecting the two stars, and we get to view this distortion from different angles as the star moves through its orbit. Photometric variations are observed as the projected area of the distorted star changes over the orbital period. Figure 7 shows a cartoon of how the changing viewing angle of a tidally distorted star produces the photometric ellipsoidal variations measured for the white dwarf binary SDSS J1054–2121 (Bell et al., 2018). There are two maxima per orbital period (ellipsoidal variation signal appears in periodograms at twice the orbital frequency), since the broad side of the star is visible twice per orbit. One maximum is higher than the other because of Doppler beaming of light in the direction ahead of the primary star’s motion (the Doppler beaming signal appears at the orbital frequency; Zucker et al., 2007). The ellipsoidal variations provide an opportunity to break the $\sin(i)$ degeneracy from orbital inclination angle that limits our understanding of most non-eclipsing binary systems, and when analyzed with other data, they can constrain the mass–radius relationship for distorted white dwarfs.

White dwarfs are quite compact and therefore must be in very close binary systems for ellipsoidal variations to be significant. In fact, this effect is most often observed from “extremely low mass” (ELM; $\lesssim 0.25 M_{\odot}$) white dwarfs. From single-star evolution, white dwarfs of such low mass are expected to form from stars with main sequence lifetimes that exceed the age of the Milky Way (Kilic et al., 2007). The ELM white dwarfs that we observe are expected to have formed through mass loss in tight binary systems, which is supported by the high fraction observed to still be in short-period binaries (Marsh et al., 1995; Brown et al., 2016). Since less massive white dwarfs have larger radii, the ELM white dwarfs are more deformable, and since most are in tight binary systems, many ELM white dwarfs exhibit ellipsoidal variations. Analyzing the ellipsoidal variation signatures can constrain the properties of the ELM white dwarfs and their binary companions, and can provide insights into their evolutionary pathways through binary mass transfer (Hermes et al., 2014).

5 Conclusions

The photometric variability of white dwarf stars can provide valuable insights into the physical properties of these compact stellar remnants. Stellar pulsations in particular can be used to constrain white dwarf interior structures, especially those with many modes that propagate in different regions within these stars. Brightness variations from rotation or photometric binaries typically appear at rotation/orbital frequencies and/or harmonics of these frequencies; these scenarios can be difficult to tell apart in some cases from photometry alone, but close binaries will show radial velocity variations in spectroscopic data with a consistent periodicity.

Recent and planned astronomical surveys are increasingly collecting photometric data in the time domain, revealing an abundance of variable white dwarf systems. The ideal light curves for unambiguous characterization of variability are continuous, with a rapid frame rate, recorded over a long time baseline, such as those collected from the *Kepler* and *TESS* missions. Recent studies of white dwarfs have benefited tremendously from

precision astrometry from *Gaia* (Gaia Collaboration et al., 2016), which has recently revealed hundreds of thousands of white dwarf stars with significant parallaxes (Gentile Fusillo et al., 2021). Most white dwarfs brighter than an apparent *Gaia* magnitude of $G \approx 20$ have now been identified, informing efforts to discover and characterize variable white dwarfs.

Acknowledgments

Thank you to the following authors for agreeing to allow their figures to be reproduced in this chapter: J. J. Hermes, M. H. Montgomery, Zs. Bognár, and S. O. Kepler.

References

- Aerts C, Christensen-Dalsgaard J and Kurtz DW (2010). Asteroseismology. doi:10.1007/978-1-4020-5803-5.
- Andryushin AS and Popov SB (2021), Apr. Exoplanet Population Synthesis with Account for Orbit Variation Due to Stellar Evolution. *Astronomy Reports* 65 (4): 246–268. doi:10.1134/S1063772921040016. 2309.12635.
- Bell KJ, Hermes JJ, Bischoff-Kim A, Moorhead S, Montgomery MH, Østensen R, Castanheira BG and Winget DE (2015), Aug. KIC 4552982: Outbursts and Asteroseismology from the Longest Pseudo-continuous Light Curve of a ZZ Ceti. *ApJ* 809 (1), 14. doi:10.1088/0004-637X/809/1/14. 1506.07878.
- Bell KJ, Hermes JJ, Montgomery MH, Gentile Fusillo NP, Raddi R, Gänsicke BT, Winget DE, Denny E, Gianninas A, Tremblay PE, Chote P and Winget KI (2016), Oct. Outbursts in Two New Cool Pulsating DA White Dwarfs. *ApJ* 829 (2), 82. doi:10.3847/0004-637X/829/2/82. 1607.01392.
- Bell KJ, Hermes JJ and Kusztewicz JS (2018), Jul., Constraining Low-Mass White Dwarf Binaries from Ellipsoidal Variations, Castanheira B, Vanderbosch Z and Montgomery M, (Eds.), 21st European White Dwarf Workshop, arXiv:1809.05623.
- Bellm EC, Kulkarni SR, Graham MJ, Dekany R, Smith RM, Riddle R, Masci FJ, Helou G, Prince TA, Adams SM, Barbarino C, Barlow T, Bauer J, Beck R, Belicki J, Biswas R, Blagorodnova N, Bodewits D, Bolin B, Brinnel V, Brooke T, Bue B, Bulla M, Burruss R, Cenko SB, Chang CK, Connolly A, Coughlin M, Cromer J, Cunningham V, De K, Delacroix A, Desai V, Duev DA, Eadie G, Farnham TL, Feeney M, Feindt U, Flynn D, Frankowski A, Frederick S, Fremling C, Gal-Yam A, Gezari S, Giomi M, Goldstein DA, Golkhou VZ, Goobar A, Groom S, Hacopians E, Hale D, Henning J, Ho AYQ, Hover D, Howell J, Hung T, Huppenkothen D, Imel D, Ip WH, Ivezić Ž, Jackson E, Jones L, Juric M, Kasliwal MM, Kaspi S, Kaye S, Kelley MSP, Kowalski M, Kramer E, Kupfer T, Landry W, Laher RR, Lee CD, Lin HW, Lin ZY, Lunnan R, Giomi M, Mahabal A, Mao P, Miller AA, Monkewitz S, Murphy P, Ngeow CC, Nordin J, Nugent P, Ofek E, Patterson MT, Penprase B, Porter M, Rauch L, Rebbapragada U, Reiley D, Rigault M, Rodriguez H, van Roestel J, Rusholme B, van Santen J, Schulze S, Shupe DL, Singer LP, Soumagnac MT, Stein R, Surace J, Sollerman J, Szkody P, Taddia F, Terek S, Van Sistine A, van Velzen S, Vestrand WT, Walters R, Ward C, Ye QZ, Yu PC, Yan L and Zolkower J (2019), Jan. The Zwicky Transient Facility: System Overview, Performance, and First Results. *PASP* 131 (995): 018002. doi:10.1088/1538-3873/aacbbe. 1902.01932.
- Bergeron P, Fontaine G, Billères M, Boudreault S and Green EM (2004), Jan. On the Purity of the ZZ Ceti Instability Strip: Discovery of More Pulsating DA White Dwarfs on the Basis of Optical Spectroscopy. *ApJ* 600 (1): 404–408. doi:10.1086/379808. astro-ph/0309483.
- Bognár Z and Sódor Á (2024), Apr. Rotation of ZZ Ceti stars as seen by TESS. *A&A* 684, A76. doi:10.1051/0004-6361/202348759. 2402.09869.
- Bohlin RC (2014), Jun. Hubble Space Telescope CALSPEC Flux Standards: Sirius (and Vega). *AJ* 147 (6), 127. doi:10.1088/0004-6256/147/6/127.
- Bohlin RC, Gordon KD, Rieke GH, Ardila D, Carey S, Deustua S, Engelbracht C, Ferguson HC, Flanagan K, Kalirai J, Meixner M, Noriega-Crespo A, Su KYL and Tremblay PE (2011), May. Absolute Flux Calibration of the IRAC Instrument on the Spitzer Space Telescope Using Hubble Space Telescope Flux Standards. *AJ* 141 (5), 173. doi:10.1088/0004-6256/141/5/173. 1103.3469.
- Borucki WJ, Koch D, Basri G, Batalha N, Brown T, Caldwell D, Caldwell J, Christensen-Dalsgaard J, Cochran WD, DeVore E, Dunham EW, Dupree AK, Gautier TN, Geary JC, Gilliland R, Gould A, Howell SB, Jenkins JM, Kondo Y, Latham DW, Marcy GW, Meibom S, Kjeldsen H, Lissauer JJ, Monet DG, Morrison D, Sasselov D, Tarter J, Boss A, Brownlee D, Owen T, Buzasi D, Charbonneau D, Doyle L, Fortney J, Ford EB, Holman MJ, Seager S, Steffen JH, Welsh WF, Rowe J, Anderson H, Buchhave L, Ciardi D, Walkowicz L, Sherry W, Horch E, Isaacson H, Everett ME, Fischer D, Torres G, Johnson JA, Endl M, MacQueen P, Bryson ST, Dotson J, Haas M, Kolodziejczak J, Van Cleve J, Chandrasekaran H, Twicken JD, Quintana EV, Clarke BD, Allen C, Li J, Wu H, Tenenbaum P, Verner E, Bruhweiler F, Barnes J and Prsa A (2010), Feb. Kepler Planet-Detection Mission: Introduction and First Results. *Science* 327 (5968): 977. doi:10.1126/science.1185402.
- Brickhill AJ (1991), Aug. The pulsations of ZZ Ceti stars. III. The driving mechanism. *MNRAS* 251: 673–680. doi:10.1093/mnras/251.4.673.
- Brickhill AJ (1992), Dec. The pulsations of ZZ Ceti stars - V. The light curves. *MNRAS* 259: 519–528. doi:10.1093/mnras/259.3.519.
- Brown WR, Gianninas A, Kilic M, Kenyon SJ and Allende Prieto C (2016), Feb. The ELM Survey. VII. Orbital Properties of Low-Mass White Dwarf Binaries. *ApJ* 818 (2), 155. doi:10.3847/0004-637X/818/2/155. 1604.04268.
- Castanheira BG, Kepler SO, Costa AFM, Giovannini O, Robinson EL, Winget DE, Kleinman SJ, Nitta A, Eisenstein D, Koester D and Santos MG (2007), Feb. Towards a pure ZZ Ceti instability strip. *A&A* 462 (3): 989–993. doi:10.1051/0004-6361:20065886. astro-ph/0611332.
- Castanheira BG, Kepler SO, Kleinman SJ, Nitta A and Fraga L (2013), Mar. Discovery of five new massive pulsating white dwarf stars. *MNRAS* 430 (1): 50–59. doi:10.1093/mnras/sts474.
- Córsico AH, Althaus LG, Benvenuto OG and Serenelli AM (2002), May. The mode trapping properties of full DA white dwarf evolutionary models. *A&A* 387: 531–549. doi:10.1051/0004-6361:20020384. astro-ph/0203453.
- Córsico AH, Uzundag M, Kepler SO, Althaus LG, Silvotti R, Bradley PA, Baran AS, Koester D, Bell KJ, Romero AD, Hermes JJ and Gentile Fusillo NP (2022), Dec. Pulsating hydrogen-deficient white dwarfs and pre-white dwarfs observed with TESS. V. Discovery of two new DBV pulsators, WDJ152738.4–450207.4 and WD 1708–871, and asteroseismology of the already known DBV stars PG 1351+489, EC 20058–5234, and EC 04207–4748. *A&A* 668, A161. doi:10.1051/0004-6361/202244198. 2210.05486.
- Costa JES and Kepler SO (2008), Oct. The temporal changes of the pulsational periods of the pre-white dwarf PG 1159-035. *A&A* 489 (3): 1225–1232. doi:10.1051/0004-6361:20079118. 0807.5137.
- Dupuis J, Chayer P, Vennes S, Christian DJ and Kruk JW (2000), Jul. Adding More Mysteries to the DA White Dwarf GD 394. *ApJ* 537 (2): 977–992. doi:10.1086/309079.
- Dziembowski W (1977), Jan. Light and radial velocity variations in a nonradially oscillating star. *AcA* 27: 203–211.

- Fontaine G, Brassard P and Bergeron P (2001), Apr. The Potential of White Dwarf Cosmochronology. *PASP* 113 (782): 409–435. doi:10.1086/319535.
- Gaia Collaboration, Prusti T, de Bruijne JHJ, Brown AGA, Vallenari A, Babusiaux C, Bailer-Jones CAL, Bastian U, Biermann M, Evans DW, Eyler L, Jansen F, Jordi C, Klioner SA, Lammars U, Lindegren L, Luri X, Mignard F, Milligan DJ, Panem C, Poinsignon V, Pourbaix D, Randich S, Sarri G, Sartoretti P, Siddiqui HI, Soubiran C, Valette V, van Leeuwen F, Walton NA, Aerts C, Arenou F, Cropper M, Drimmel R, Høg E, Katz D, Lattanzi MG, O'Mullane W, Grebel EK, Holland AD, Huc C, Passot X, Bramante L, Cacciari C, Castañeda J, Chaoul L, Cheek N, De Angeli F, Fabricius C, Guerra R, Hernández J, Jean-Antoine-Piccolo A, Masana E, Messineo R, Mowlavi N, Nienartowicz K, Ordóñez-Blanco D, Panuzzo P, Portell J, Richards PJ, Riello M, Seabroke GM, Tanga P, Thévenin F, Torra J, Els SG, Gracia-Abril G, Comoretto G, García-Reinaldos M, Lock T, Mercier E, Altmann M, Andrae R, Blaauw TL, Bellas-Verdís I, Benson K, Berthier J, Blomme R, Busso G, Carry B, Cellino A, Clementini G, Cowell S, Creevey O, Cuypers J, Davidson M, De Ridder J, de Torres A, Delchambre L, Dell'Oro A, Ducourant C, Frémat Y, García-Torres M, Gosset E, Halbwegs JL, Hambly NC, Harrison DL, Hauser M, Hestroffer D, Hodgkin ST, Huckle HE, Hutton A, Jasniewicz G, Jordan S, Kontizas M, Korn AJ, Lanzafame AC, Manteiga M, Moitinho A, Muinonen K, Osinde J, Pancino E, Pauwels T, Petit JM, Recio-Blanco A, Robin AC, Sarro LM, Siopis C, Smith M, Smith KW, Sozzetti A, Thuillot W, van Reeven W, Viala Y, Abbas U, Abreu Aramburu A, Accart S, Aguado JJ, Allan PM, Allasia W, Altavilla G, Álvarez MA, Alves J, Anderson RI, Andrei AH, Anglada Varela E, Antiche E, Antoja T, Antón S, Arcay B, Atzei A, Ayache L, Bach N, Baker SG, Balaguer-Núñez L, Barache C, Barata C, Barbier A, Barblan F, Baroni M, Barrado y Navascués D, Barros M, Barstow MA, Becciani U, Bellazzini M, Bellei G, Bello García A, Belokurov V, Bendjoya P, Berihuete A, Bianchi L, Bienaymé O, Billebaud F, Blagorodnova M, Blanco-Cuaresma S, Boch T, Bombrun A, Borrachero R, Bouquillon S, Bourda G, Bouy H, Bragaglia A, Breddels MA, Brouillet N, Brūsemeister T, Bucciarelli B, Budnik F, Burgess P, Burgon R, Burlacu A, Busonero D, Buzzì R, Caffau E, Cambras J, Campbell H, Cancelliere R, Cantat-Gaudin T, Carlucci T, Carrasco JM, Castellani M, Charlot P, Charnas J, Charvet P, Chassat F, Chiavassa A, Clotet M, Cocozza G, Collins RS, Collins P, Costigan G, Crifo F, Cross NJG, Crosta M, Crowley C, Dafonte C, Damerdy J, Dapergolas A, David P, David M, De Cat P, de Felice F, de Laverny P, De Luise F, De March R, de Martino D, de Souza R, Debusscher J, del Pozo E, Delbo M, Delgado A, Delgado HE, di Marco F, Di Matteo P, Diakite S, Distefano E, Dolding C, Dos Anjos S, Drazinos P, Durán J, Dzigan Y, Ecale E, Edvardsson B, Enke H, Erdmann M, Escolar D, Espina M, Evans NW, Eynard Bontemps G, Fabre C, Fabrizio M, Faigler S, Falcão AJ, Farrás Casas M, Faye F, Federici L, Fedorets G, Fernández-Hernández J, Fernique P, Fienng A, Figueras F, Filippi F, Findeisen K, Fonti A, Fouesneau M, Fraile E, Fraser M, Fuchs J, Furnell R, Gai M, Galletti S, Galluccio L, Garabato D, García-Sedano F, Garé P, Garofalo A, Garralda N, Gavras P, Gerssen J, Geyer R, Gilmore G, Girona S, Giuffrida G, Gomes M, González-Marcos A, González-Núñez J, González-Vidal JJ, Granvik M, Guerrier A, Guillout P, Guiraud J, Gúrpide A, Gutiérrez-Sánchez R, Guy LP, Haigron R, Hatzidimitriou D, Haywood M, Heiter U, Helmi A, Hobbs D, Hofmann W, Holl B, Holland G, Hunt JAS, Hupki A, Icardi V, Irwin M, Jevardat de Fombelle G, Jofré P, Jonker PG, Jorissen A, Julbe F, Karampelas A, Kochoska A, Kohley R, Kolenberg K, Kontizas E, Koposov SE, Kordopatis G, Koubzky P, Kowalczyk A, Krone-Martins A, Kudryashova M, Kull I, Bachchan RK, Lacoste-Seris F, Lanza AF, Lavigne JB, Le Poncin-Lafitte C, Lebreton Y, Lebzelter T, Leccia S, Leclerc N, Lecoœur-Taibi I, Lemaitre V, Lenhardt H, Leroux F, Liao S, Licata E, Lindstrøm HEP, Lister TA, Livanou E, Lobel A, Löffler W, López M, Lopez-Lozano A, Lorenz D, Loureiro T, MacDonald I, Magalhães Fernandes T, Managau S, Mann RG, Mantelet G, Marchal O, Marchant JM, Marconi M, Marie J, Marinoni S, Marrese PM, Marschall G, Marshall DJ, Martín-Fleitas JM, Martino M, Mary N, Matijević G, Mazeh T, McMillan PJ, Messina S, Mestre A, Michalik D, Millar NR, Miranda BMH, Molina D, Molinaro R, Molinaro M, Molnár L, Moniez M, Montegriffo P, Monteiro D, Mor R, Mora A, Morbidelli R, Morel T, Morgenthaler S, Morley T, Morris D, Mulone AF, Muraveva T, Musella I, Narbonne J, Nelemans G, Nicastro L, Noval L, Ordénovic C, Odiéres-Meré J, Osborne P, Pagani C, Pagano I, Pailler F, Palacin H, Palaversa L, Parsons P, Paulsen T, Pecoraro M, Pedrosa R, Pentikäinen H, Pereira J, Pichon B, Piersimoni AM, Pineau FX, Plachy E, Plum G, Poujoulet E, Prša A, Pulone L, Ragaini S, Rago S, Rambaux N, Ramos-Lerate M, Ranalli P, Rauw G, Read A, Regibo S, Renk F, Reylé C, Ribeiro RA, Rimoldini L, Ripepi V, Riva A, Rixon G, Roelens M, Romero-Gómez M, Rowell N, Royer F, Rudolph A, Ruiz-Dern L, Sadowski G, Sagristá Sellés T, Sahlmann J, Salgado J, Salguero E, Sarasso M, Savietto H, Schnorhk A, Schultheis M, Sciacca E, Segol M, Segovia JC, Segransan D, Serpell E, Shih IC, Smareglia R, Smart RL, Smith C, Solano E, Solitto F, Sordo R, Soria Nieto S, Souchay J, Spagna A, Spoto F, Stampa U, Steele IA, Steidelmüller H, Stephenson CA, Stoev H, Suess FF, Süveges M, Surdej J, Szabados L, Szegedi-Elek E, Tapiador D, Taris F, Tauran G, Taylor MB, Teixeira R, Terrett D, Tingley B, Trager SC, Turon C, Ulla A, Utrilla E, Valentini G, van Elteren A, Van Hemelryck E, van Leeuwen M, Varadi M, Vecchiato A, Veljanoski J, Via T, Vicente D, Vogt S, Voss H, Votrubá V, Voutsinas S, Walmsley G, Weiler M, Weingrill K, Werner D, Wevers T, Whitehead G, Wyrzykowski Ł, Yoldas A, Žerjal M, Zucker S, Zurbach C, Zwitter T, Alecu A, Allen M, Allende Prieto C, Amorim A, Anglada-Escudé G, Arsenijević V, Azaz S, Balm P, Beck M, Bernstein HH, Bigot L, Bijaoui A, Blasco C, Bonfigli M, Bono G, Boudreault S, Bressan A, Brown S, Brunet PM, Bunclark P, Buonanno R, Butkevich AG, Carret C, Carrion C, Chemin L, Chéreau F, Corcione L, Darmigny E, de Boer KS, de Teodoro P, de Zeeuw PT, Delle Lucche C, Domingues CD, Dubath P, Fodor F, Frézouls B, Fries A, Fustes D, Fyfe D, Gallardo E, Gallegos J, Gardiol D, Gebran M, Gomboc A, Gómez A, Grux E, Gueguen A, Heyrovsky A, Hoar J, Iannicola G, Isasi Parache Y, Janotto AM, Joliet E, Jonckheere A, Keil R, Kim DW, Klagyivik P, Klar J, Knude J, Kochukhov O, Kolka I, Kos J, Kutka A, Lainey V, LeBouquin D, Liu C, Loreggia D, Makarov VV, Marseille MG, Martayan C, Martínez-Rubi O, Massart B, Meynadier F, Mignot S, Munari U, Nguyen AT, Nordlander T, Ocirk P, O'Flaherty KS, Olias Sanz A, Ortiz P, Osorio J, Oszkiewicz D, Ouzounis A, Palmer M, Park P, Pasquato E, Peltzer C, Peralta J, Péturard F, Pieniluoma T, Pigozzi E, Poels J, Prat G, Prod'homme T, Raison F, Rebordao JM, Risqueuz D, Rocca-Volmerange B, Rosen S, Ruiz-Fuertes MI, Russo F, Sembay S, Serraller Vizcaino I, Short A, Siebert A, Silva H, Sinachopoulos D, Slezak E, Soffel M, Sosnowska D, Straizys V, ter Linden M, Terrell D, Theil S, Tiede C, Troisi L, Tsalmantza P, Tur D, Vaccari M, Vachier F, Valles P, Van Hamme W, Veltz L, Virtanen J, Wallut JM, Wichmann R, Wilkinson MI, Ziaeeppour H and Zschocke S (2016), Nov. The Gaia mission. *A&A* 595, A1. doi:10.1051/0004-6361/201629272. 1609.04153.
- Gautschy A, Althaus LG and Saio H (2005), Aug. On the excitation of PG 1159-type pulsations. *A&A* 438 (3): 1013–1020. doi:10.1051/0004-6361:20042486. astro-ph/0504495.
- Gentile Fusillo NP, Tremblay PE, Cukanovaite E, Vorontseva A, Lallement R, Hollands M, Gänsicke BT, Burdge KB, McCleery J and Jordan S (2021), Dec. A catalogue of white dwarfs in Gaia EDR3. *MNRAS* 508 (3): 3877–3896. doi:10.1093/mnras/stab2672. 2106.07669.
- Giammichele N, Charpinet S and Brassard P (2022), Jun. Seismic Cartography of White-Dwarf Interiors From the Toulouse-Montréal Optimal-Design Approach. *Frontiers in Astronomy and Space Sciences* 9, 879045. doi:10.3389/fspas.2022.879045.
- Goldreich P and Wu Y (1999), Feb. Gravity Modes in ZZ Ceti Stars. I. Quasi-adiabatic Analysis of Overstability. *ApJ* 511 (2): 904–915. doi:10.1086/306705. astro-ph/9804305.
- Hardy F, Dufour P and Jordan S (2023), Apr. Spectrophotometric analysis of magnetic white dwarf - I. Hydrogen-rich compositions. *MNRAS* 520 (4): 6111–6134. doi:10.1093/mnras/stad196. 2301.06596.
- Hermes JJ, Montgomery MH, Gianninas A, Winget DE, Brown WR, Harrold ST, Bell KJ, Kenyon SJ, Kilic M and Castanheira BG (2013), Dec. A new class of pulsating white dwarf of extremely low mass: the fourth and fifth members. *MNRAS* 436 (4): 3573–3580. doi:10.1093/mnras/stt1835. 1310.0013.
- Hermes JJ, Brown WR, Kilic M, Gianninas A, Chote P, Sullivan DJ, Winget DE, Bell KJ, Falcon RE, Winget KI, Mason PA, Harrold ST and Montgomery MH (2014), Sep. Radius Constraints from High-speed Photometry of 20 Low-mass White Dwarf Binaries. *ApJ* 792 (1), 39.

- doi:10.1088/0004-637X/792/1/39. 1407.3798.
- Hermes JJ, Montgomery MH, Bell KJ, Chote P, Gänsicke BT, Kawaler SD, Clemens JC, Dunlap BH, Winget DE and Armstrong DJ (2015), Sep. A Second Case of Outbursts in a Pulsating White Dwarf Observed by Kepler. *ApJL* 810 (1), L5. doi:10.1088/2041-8205/810/1/L5. 1507.06319.
- Hermes JJ, Gänsicke BT, Gentile Fusillo NP, Raddi R, Hollands MA, Dennihy E, Fuchs JT and Redfield S (2017a), Jun. When flux standards go wild: white dwarfs in the age of Kepler. *MNRAS* 468 (2): 1946–1952. doi:10.1093/mnras/stx567. 1703.02048.
- Hermes JJ, Gänsicke BT, Kawaler SD, Greiss S, Tremblay PE, Gentile Fusillo NP, Raddi R, Fanale SM, Bell KJ, Dennihy E, Fuchs JT, Dunlap BH, Clemens JC, Montgomery MH, Winget DE, Chote P, Marsh TR and Redfield S (2017b), Oct. White Dwarf Rotation as a Function of Mass and a Dichotomy of Mode Line Widths: Kepler Observations of 27 Pulsating DA White Dwarfs through K2 Campaign 8. *ApJS* 232 (2), 23. doi:10.3847/1538-4365/aa8bb5. 1709.07004.
- Howell SB, Sobeck C, Haas M, Still M, Barclay T, Mullally F, Troeltzsch J, Aigrain S, Bryson ST, Caldwell D, Chaplin WJ, Cochran WD, Huber D, Marcy GW, Miglio A, Najita JR, Smith M, Twicken JD and Fortney JJ (2014), Apr. The K2 Mission: Characterization and Early Results. *PASP* 126 (938): 398. doi:10.1086/676406. 1402.5163.
- Isern J, Torres S and Rebassa-Mansergas A (2022), Jan. White dwarfs as Physics laboratories: lights and shadows. *Frontiers in Astronomy and Space Sciences* 9, 6. doi:10.3389/fspas.2022.815517. 2202.02052.
- Kalirai JS, Hansen BMS, Kelson DD, Reitzel DB, Rich RM and Richer HB (2008), Mar. The Initial-Final Mass Relation: Direct Constraints at the Low-Mass End. *ApJ* 676 (1): 594–609. doi:10.1086/527028. 0706.3894.
- Kawaler SD (1988), Jan., The Stellar Seismology of the Hot White Dwarf Star PG:1159-035, Christensen-Dalsgaard J and Frandsen S, (Eds.), *Advances in Helio- and Asteroseismology*, 123, pp. 329.
- Kepler SO, Robinson EL, Nather RE and McGraw JT (1982), Mar. The pulsating white dwarf G 117-B15A. *ApJ* 254: 676–682. doi:10.1086/159779.
- Kepler SO, Nather RE, Winget DE, Nitta A, Kleinman SJ, Metcalfe T, Sekiguchi K, Jiang X, Sullivan D, Sullivan T, Janulis R, Meistas E, Kalytis R, Krzesinski J, Ogoza W, Zola S, O'Donoghue D, Romero-Colmenero E, Martinez P, Dreizler S, Deetjen J, Nagel T, Schuh SL, Vaclair G, Ning FJ, Chevreton M, Solheim JE, Gonzalez Perez JM, Johannessen F, Kanaan A, Costa JE, Murillo Costa AF, Wood MA, Silvestri N, Ahrens TJ, Jones AK, Collins AE, Boyer M, Shaw JS, Mukadam A, Klumpe EW, Larrison J, Kawaler S, Riddle R, Ulla A and Bradley P (2003), Apr. The everchanging pulsating white dwarf GD358. *A&A* 401: 639–654. doi:10.1051/0004-6361:20030105. astro-ph/03011477.
- Kepler SO, Winget DE, Vanderbosch ZP, Castanheira BG, Hermes JJ, Bell KJ, Mullally F, Romero AD, Montgomery MH, DeGennaro S, Winget KI, Chandler D, Jeffery EJ, Fritzen JK, Williams KA, Chote P and Zola S (2021), Jan. The Pulsating White Dwarf G117-B15A: Still the Most Stable Optical Clock Known. *ApJ* 906 (1), 7. doi:10.3847/1538-4357/abc626. 2010.16062.
- Kilic M, Stanek KZ and Pinsonneault MH (2007), Dec. The Future Is Now: The Formation of Single Low-Mass White Dwarfs in the Solar Neighborhood. *ApJ* 671 (1): 761–766. doi:10.1086/522228. 0706.3045.
- Kilic M, Córscico AH, Moss AG, Jewett G, De Gerónimo FC and Althaus LG (2023), Jun. WD J004917.14-252556.81: the most massive pulsating white dwarf. *MNRAS* 522 (2): 2181–2187. doi:10.1093/mnras/stad1113. 2304.10330.
- Kleinman SJ, Nather RE, Winget DE, Clemens JC, Bradley PA, Kanaan A, Provencal JL, Claver CF, Watson TK, Yanagida K, Nitta A, Dixon JS, Wood MA, Grauer AD, Hine BP, Fontaine G, Liebert J, Sullivan DJ, Wickramasinghe DT, Achilles N, Marar TMK, Seetha S, Ashoka BN, Meištās E, Leibowitz EM, Moskalik P, Krześciński J, Solheim JE, Bruvold A, O'Donoghue D, Kurtz DW, Warner B, Martinez P, Vaclair G, Dolez N, Chevreton M, Barstow MA, Kepler SO, Giovannini O, Augusteijn T, Hansen CJ and Kawaler SD (1998), Mar. Understanding the Cool DA White Dwarf Pulsator, G29-38. *ApJ* 495 (1): 424–434. doi:10.1086/305259. astro-ph/9711123.
- Kochanek CS, Shappee BJ, Stanek KZ, Holoien TWS, Thompson TA, Prieto JL, Dong S, Shields JV, Will D, Britt C, Perzanowski D and Pojmański G (2017), Oct. The All-Sky Automated Survey for Supernovae (ASAS-SN) Light Curve Server v1.0. *PASP* 129 (980): 104502. doi:10.1088/1538-3873/aa80d9. 1706.07060.
- Kruse E and Agol E (2014), Apr. KOI-3278: A Self-Lensing Binary Star System. *Science* 344 (6181): 275–277. doi:10.1126/science.1251999. 1404.4379.
- Kunimoto M and Matthews JM (2020), Jun. Searching the Entirety of Kepler Data. II. Occurrence Rate Estimates for FGK Stars. *AJ* 159 (6), 248. doi:10.3847/1538-3881/ab88b0. 2004.05296.
- Lasker BM and Hesser JE (1971), Feb. High-Frequency Stellar Oscillations. VI. R548, a Periodically Variable White Dwarf. *ApJL* 163: L89. doi:10.1086/180673.
- Ledoux P (1951), Jan. Sur la stabilité gravitationnelle d'une nébuleuse isotherme. *Annales d'Astrophysique* 14: 438.
- LSST Science Collaboration, Abell PA, Allison J, Anderson SF, Andrew JR, Angel JRP, Armus L, Arnett D, Asztalos SJ, Axelrod TS, Bailey S, Ballantyne DR, Bankert JR, Barkhouse WA, Barr JD, Barrientos LF, Barth AJ, Bartlett JG, Becker AC, Becla J, Beers TC, Bernstein JP, Biswas R, Blanton MR, Bloom JS, Bochanski JJ, Boeshaar P, Borne KD, Bradac M, Brandt WN, Bridge CR, Brown ME, Brunner RJ, Bullock JS, Burgasser AJ, Burge JH, Burke DL, Cargile PA, Chandrasekharan S, Chartas G, Chesley SR, Chu YH, Cinabro D, Claire MW, Claver CF, Clowe D, Connolly AJ, Cook KH, Cooke J, Cooray A, Covey KR, Culliton CS, de Jong R, de Vries WH, Debattista VP, Delgado F, Dell'Antonio IP, Dhital S, Di Stefano R, Dickinson M, Dilday B, Djorgovski SG, Dobler G, Donalek C, Dubois-Felsmann G, Durech J, Eliasdottir A, Eracleous M, Eyer L, Falco EE, Fan X, Fassnacht CD, Ferguson HC, Fernandez YR, Fields BD, Finkbeiner D, Figueroa EE, Fox DB, Francke H, Frank JS, Frieman J, Fromenteau S, Furqan M, Galaz G, Gal-Yam A, Garnavich P, Gawiser E, Geary J, Gee P, Gibson RR, Gilmore K, Grace EA, Green RF, Gressler WJ, Grillmair CJ, Habib S, Haggerty JS, Hamuy M, Harris AW, Hawley SL, Heavens AF, Hebb L, Henry TJ, Hileman E, Hilton EJ, Hoadley K, Holberg JB, Holman MJ, Howell SB, Infante L, Ivezić Z, Jacoby SH, Jain B, R, Jedicke, Jee MJ, Garrett Hernigan J, Jha SW, Johnston KV, Jones RL, Juric M, Kaasalainen M, Styliani, Kafka, Kahn SM, Kaib NA, Kalirai J, Kantor J, Kasliwal MM, Keeton CR, Kessler R, Knezevic Z, Kowalski A, Krabbendam VL, Krughoff KS, Kulkarni S, Kuhlman S, Lacy M, Lepine S, Liang M, Lien A, Lira P, Long KS, Lorenz S, Lotz JM, Lupton RH, Lutz J, Macri LM, Mahabal AA, Mandelbaum R, Marshall P, May M, McGehee PM, Meadows BT, Meert A, Milani A, Miller CJ, Miller M, Mills D, Minniti D, Monet D, Mukadam AS, Nakar E, Neill DR, Newman JA, Nikolaev S, Nordby M, O'Connor P, Oguri M, Oliver J, Olivier SS, Olsen JK, Olsen K, Olszewski EW, Oluseyi H, Padilla ND, Parker A, Pepper J, Peterson JR, Petry C, Pinto PA, Pizagno JL, Popescu B, Prsa A, Radcka V, Raddick MJ, Rasmussen A, Rau A, Rho J, Rhoads JE, Richards GT, Ridgway ST, Robertson BE, Roskar R, Saha A, Sarajedini A, Scannapieco E, Schalk T, Schindler R, Schmidt S, Schmidt S, Schneider DP, Schumacher G, Scranton R, Sebag J, Seppala LG, Shemmer O, Simon JD, Sivertz M, Smith HA, Allyn Smith J, Smith N, Spitz AH, Stanford A, Stassun KG, Strader J, Strauss MA, Stubbins CW, Sweeney DW, Szalay A, Szkody P, Takada M, Thorman P, Trilling DE, Trimble V, Tyson A, Van Berg R, Vanden Berk D, VanderPlas J, Verde L, Vrsnak B, Walkowicz LM, Wandelt BD, Wang S, Wang Y, Warner M, Wechsler RH, West AA, Wiecha O, Williams BF, Willman B, Wittman D, Wolff SC, Wood-Vasey WM, Wozniak P, Young P, Zentner A and Zhan H (2009), Dec. LSST Science Book, Version 2.0. *arXiv e-prints*, arXiv:0912.0201doi:10.48550/arXiv.0912.0201. 0912.0201.
- Luan J and Goldreich P (2018), Aug. DAVs: Red Edge and Outbursts. *ApJ* 863 (1), 82. doi:10.3847/1538-4357/aad0f4. 1711.06367.
- Marsh TR, Dhillion VS and Duck SR (1995), Aug. Low-Mass White Dwarfs Need Friends - Five New Double-Degenerate Close Binary Stars. *MNRAS* 275: 828. doi:10.1093/mnras/275.3.828.
- Montgomery MH (2005a), Nov. A New Technique for Probing Convection in Pulsating White Dwarf Stars. *ApJ* 633 (2): 1142–1149.

- doi:10.1086/466511. astro-ph/0507444.
- Montgomery MH (2005b), Jul., The Vibrating String Analogy and Mode Trapping, Koester D and Moehler S, (Eds.), 14th European Workshop on White Dwarfs, Astronomical Society of the Pacific Conference Series, 334, pp. 553.
- Montgomery MH, Hermes JJ, Winget DE, Dunlap BH and Bell KJ (2020), Feb. Limits on Mode Coherence in Pulsating DA White Dwarfs Due to a Nonstatic Convection Zone. *ApJ* 890 (1), 11. doi:10.3847/1538-4357/ab6a0e. 2001.05048.
- Mukadam AS, Montgomery MH, Winget DE, Kepler SO and Clemens JC (2006), Apr. Ensemble Characteristics of the ZZ Ceti Stars. *ApJ* 640 (2): 956–965. doi:10.1086/500289. astro-ph/0507425.
- Mukadam AS, Bischoff-Kim A, Fraser O, Córscico AH, Montgomery MH, Kepler SO, Romero AD, Winget DE, Hermes JJ, Riecken TS, Kronberg ME, Winget KI, Falcon RE, Chandler DW, Kuehne JW, Sullivan DJ, Reaves D, von Hippel T, Mullally F, Shipman H, Thompson SE, Silvestri NM and Hynes RI (2013), Jul. Measuring the Evolutionary Rate of Cooling of ZZ Ceti. *ApJ* 771 (1), 17. doi:10.1088/0004-637X/771/1/17.
- Mullally F, Winget DE, Degennaro S, Jeffery E, Thompson SE, Chandler D and Kepler SO (2008), mar. Limits on planets around pulsating white dwarf stars. *The Astrophysical Journal* 676 (1): 573. doi:10.1086/528672. <https://dx.doi.org/10.1086/528672>.
- Mullally SE, Sloan GC, Hermes JJ, Kunz M, Hambleton K, Bohlin R, Fleming SW, Gordon KD, Kaleida C and Mohamed K (2022), Mar. Searching for TESS Photometric Variability of Possible JWST Spectrophotometric Standard Stars. *AJ* 163 (3), 136. doi:10.3847/1538-3881/ac4bce. 2201.03670.
- Nather RE, Winget DE, Clemens JC, Hansen CJ and Hine BP (1990), Sep. The Whole Earth Telescope: A New Astronomical Instrument. *ApJ* 361: 309. doi:10.1086/169196.
- O'Donoghue D (1994), Sep. The inverse variance method for assessing measurements of dP/dt and equal-period spacings in rapid variable stars. *MNRAS* 270: 222–228. doi:10.1093/mnras/270.2.222.
- Provencal JL, Montgomery MH, Kanaan A, Shipman HL, Childers D, Baran A, Kepler SO, Reed M, Zhou A, Eggen J, Watson TK, Winget DE, Thompson SE, Riaz B, Nitta A, Kleinman SJ, Crowe R, Slivkoff J, Sherard P, Purves N, Binder P, Knight R, Kim SL, Chen WP, Yang M, Lin HC, Lin CC, Chen CW, Jiang XJ, Sergeev AV, Mkrtychian D, Andreev M, Janulis R, Siwak M, Zola S, Koziel D, Stachowski G, Paparo M, Bognar Z, Handler G, Lorenz D, Steininger B, Beck P, Nagel T, Kusterer D, Hoffman A, Reiff E, Kowalski R, Vauclair G, Charpinet S, Chevreton M, Solheim JE, Pakstiene E, Fraga L and Dalessio J (2009), Mar. 2006 Whole Earth Telescope Observations of GD358: A New Look at the Prototype DBV. *ApJ* 693 (1): 564–585. doi:10.1088/0004-637X/693/1/564. 0811.0768.
- Redaelli M, Kepler SO, Costa JES, Winget DE, Handler G, Castanheira BG, Kanaan A, Fraga L, Henrique P, Giovannini O, Provencal JL, Shipman HL, Dalessio J, Thompson SE, Mullally F, Brewer MM, Childers D, Oksala ME, Rosen R, Wood MA, Reed MD, Walter B, Strickland W, Chandler D, Watson TK, Nather RE, Montgomery MH, Bischoff-Kim A, Hansen CJ, Nitta A, Kleinman SJ, Claver CF, Brown TM, Sullivan DJ, Kim SL, Chen WP, Yang M, Shih CY, Zhang X, Jiang X, Fu JN, Seetha S, Ashoka BN, Marar TMK, Baliyan KS, Vats HO, Chernyshev AV, Ibbetson P, Leibowitz E, Hemar S, Sergeev AV, Andreev MV, Janulis R, Meištās EG, Moskaik P, Pajdosz G, Baran A, Winiarski M, Zola S, Ogloza W, Siwak M, Bognár Z, Solheim JE, Sefako R, Buckley D, O'Donoghue D, Nagel T, Silvotti R, Bruni I, Frey JR, Vauclair G, Chevreton M, Dolez N, Pfeiffer B, Barstow MA, Creevey OL, Kawaler SD and Clemens JC (2011), Aug. The pulsations of PG 1351+489. *MNRAS* 415 (2): 1220–1227. doi:10.1111/j.1365-2966.2011.18743.x.
- Ricker GR, Winn JN, Vanderspek R, Latham DW, Bakos GÁ, Bean JL, Berta-Thompson ZK, Brown TM, Buchhave L, Butler NR, Butler RP, Chaplin WJ, Charbonneau D, Christensen-Dalsgaard J, Clampin M, Deming D, Doty J, De Lee N, Dressing C, Dunham EW, Endl M, Fressin F, Ge J, Henning T, Holman MJ, Howard AW, Ida S, Jenkins JM, Jernigan G, Johnson JA, Kaltenegger L, Kawai N, Kjeldsen L, Laughlin G, Levine AM, Lin D, Lissauer JJ, MacQueen P, Marcy G, McCullough PR, Morton TD, Narita N, Paegert M, Palte E, Pepe F, Pepper J, Quirrenbach A, Rinehart SA, Sasselov D, Sato B, Seager S, Sozzetti A, Stassun KG, Sullivan P, Szentgyorgyi A, Torres G, Udry S and Villaseñor J (2015), Jan. Transiting Exoplanet Survey Satellite (TESS). *Journal of Astronomical Telescopes, Instruments, and Systems* 1, 014003. doi:10.1117/1.JATIS.1.1.014003.
- Riess AG, Filippenko AV, Challis P, Clocchiatti A, Diercks A, Garnavich PM, Gilliland RL, Hogan CJ, Jha S, Kirshner RP, Leibundgut B, Phillips MM, Reiss D, Schmidt BP, Schommer RA, Smith RC, Spyromilio J, Stubbs C, Suntzeff NB and Tonry J (1998), Sep. Observational Evidence from Supernovae for an Accelerating Universe and a Cosmological Constant. *AJ* 116 (3): 1009–1038. doi:10.1086/300499. astro-ph/9805201.
- Robinson E (2016). *Data Analysis for Scientists and Engineers*, Princeton University Press. ISBN 9780691169927. <https://books.google.com/books?id=6wuSjwEACAAJ>.
- Robinson EL, Kepler SO and Nather RE (1982), Aug. Multicolor variations of the ZZ CET stars. *ApJ* 259: 219–231. doi:10.1086/160162.
- Romero AD, Kepler SO, Hermes JJ, Amaral LA, Uzundag M, Bognár Z, Bell KJ, VanWyngarden M, Baran A, Pelisoli I, Oliveira GdR, Koester D, Klippel TS, Fraga L, Bradley PA, Vučković M, Heintz TM, Reding JS, Kaiser BC and Charpinet S (2022), Apr. Discovery of 74 new bright ZZ Ceti stars in the first three years of TESS. *MNRAS* 511 (2): 1574–1590. doi:10.1093/mnras/stac093. 2201.04158.
- Saio H (1996), Jan., Linear models for hydrogen-deficient star pulsations, Jeffery CS and Heber U, (Eds.), *Hydrogen Deficient Stars*, Astronomical Society of the Pacific Conference Series, 96, pp. 361.
- Saumon D, Blouin S and Tremblay PE (2022), Nov. Current challenges in the physics of white dwarf stars. *PhR* 988: 1–63. doi:10.1016/j.physrep.2022.09.001. 2209.02846.
- Sowicka P, Handler G, Jones D and van Wyk F (2021), Sep. The Missing Link? Discovery of Pulsations in the Nitrogen-rich PG 1159 Star PG 1144+005. *ApJL* 918 (1), L1. doi:10.3847/2041-8213/ac1c08. 2108.08167.
- Sowicka P, Handler G, Jones D, Caldwell JAR, van Wyk F, Paunzen E, Bąkowska K, Peralta de Arriba L, Suárez-Andrés L, Werner K, Karjalainen M and Holdsworth DL (2023), Nov. The GW Vir Instability Strip in Light of New Observations of PG 1159 Stars: Discovery of Pulsations in the Central Star of A72 and Variability of RX J0122.9-7521. *ApJS* 269 (1), 32. doi:10.3847/1538-4365/acfbc4. 2309.16537.
- Sullivan DJ and Chote P (2015), Jun., The Frequency Stability of the Pulsating White Dwarf L19-2, Dufour P, Bergeron P and Fontaine G, (Eds.), 19th European Workshop on White Dwarfs, Astronomical Society of the Pacific Conference Series, 493, pp. 199.
- Tassoul M, Fontaine G and Winget DE (1990), Feb. Evolutionary Models for Pulsation Studies of White Dwarfs. *ApJS* 72: 335. doi:10.1086/191420.
- Uzundag M, Córscico AH, Kepler SO, Althaus LG, Werner K, Reindl N and Vučković M (2022), Jun. Pulsating hydrogen-deficient white dwarfs and pre-white dwarfs observed with TESS - IV. Discovery of two new GW Vir stars: TIC 0403800675 and TIC 1989122424. *MNRAS* 513 (2): 2285–2291. doi:10.1093/mnras/stac1027. 2204.02501.
- Van Grootel V, Fontaine G, Brassard P and Dupret MA (2013), Jan. The Newly Discovered Pulsating Low-mass White Dwarfs: An Extension of the ZZ Ceti Instability Strip. *ApJ* 762 (1), 57. doi:10.1088/0004-637X/762/1/57.
- Van Grootel V, Fontaine G, Brassard P and Dupret MA (2017), Mar., The Theoretical Instability Strip of V777 Her White Dwarfs, Tremblay PE, Gaensicke B and Marsh T, (Eds.), 20th European White Dwarf Workshop, Astronomical Society of the Pacific Conference Series, 509, pp. 321.
- Vanderbosch ZP, Hermes JJ, Winget DE, Montgomery MH, Bell KJ, Nitta A and Kepler SO (2022), Mar. The Pulsating Helium-atmosphere White Dwarfs. I. New DBVs from the Sloan Digital Sky Survey. *ApJ* 927 (2), 158. doi:10.3847/1538-4357/ac4caf. 2201.09893.

- VanderPlas JT (2018), May. Understanding the Lomb-Scargle Periodogram. *ApJS* 236 (1), 16. doi:10.3847/1538-4365/aab766. 1703.09824.
- Veras D and Gänsicke BT (2015), Feb. Detectable close-in planets around white dwarfs through late unpacking. *MNRAS* 447 (2): 1049–1058. doi:10.1093/mnras/stu2475. 1411.6012.
- Winget DE, Robinson EL, Nather RD and Fontaine G (1982a), Nov. Photometric observations of GD 358 : OB white dwarfs do pulsate. *ApJL* 262: L11–L15. doi:10.1086/183902.
- Winget DE, van Horn HM, Tassoul M, Fontaine G, Hansen CJ and Carroll BW (1982b), Jan. Hydrogen-driving and the blue edge of compositionally stratified ZZ Ceti star models. *ApJL* 252: L65–L68. doi:10.1086/183721.
- Winget DE, Hansen CJ, Liebert J, van Horn HM, Fontaine G, Nather RE, Kepler SO and Lamb DQ (1987), Apr. An Independent Method for Determining the Age of the Universe. *ApJL* 315: L77. doi:10.1086/184864.
- Winget et al. (1991), Sep. Asteroseismology of the DOV star PG 1159 - 035 with the Whole Earth Telescope. *ApJ* 378: 326–346. doi:10.1086/170434.
- Winget DE, Hermes JJ, Mullally F, Bell KJ, Montgomery MH, Williams SG, Harrold ST, Kepler SO, Castanheira B, Chandler DW, Winget KI, Mukadam AS and Nather RE (2015), Jun., Limits from the Ongoing Search for Planets Around White Dwarf Stars Using Pulsation Timings, Dufour P, Bergeron P and Fontaine G, (Eds.), 19th European Workshop on White Dwarfs, Astronomical Society of the Pacific Conference Series, 493, pp. 285.
- Wu Y (2001), May. Combination frequencies in the Fourier spectra of white dwarfs. *MNRAS* 323 (1): 248–256. doi:10.1046/j.1365-8711.2001.04224.x. astro-ph/0003101.
- Wu Y and Goldreich P (1999), Jul. Gravity Modes in ZZ Ceti Stars. II. Eigenvalues and Eigenfunctions. *ApJ* 519 (2): 783–792. doi:10.1086/307412.
- Yeates CM, Clemens JC, Thompson SE and Mullally F (2005), Dec. Mode Identification from Combination Frequency Amplitudes in ZZ Ceti Stars. *ApJ* 635 (2): 1239–1262. doi:10.1086/497616. astro-ph/0511426.
- Zucker S, Mazeh T and Alexander T (2007), Dec. Beaming Binaries: A New Observational Category of Photometric Binary Stars. *ApJ* 670 (2): 1326–1330. doi:10.1086/521389. 0708.2100.